Nanotechnology

PAPER

Etch characteristics of magnetic tunnel junction materials using H_2/NH_3 reactive ion beam

To cite this article: Ju Eun Kim *et al* 2021 *Nanotechnology* **32** 055301

IOP Publishing Nanotechnology

Nanotechnology **32** (2021) 055301 (9pp) https://doi.org/10.1088/1361-6528/abb04e

Etch characteristics of magnetic tunnel junction materials using H_2/NH_3 reactive ion beam

Ju Eun Kim[1], Doo San Kim[1], You Jung Gill[1], Yun Jong Jang[1], Ye Eun Kim[1], Hanna Cho[3], Bok-Yeon Won[3], Oik Kwon[3], Kukhan Yoon[3], Jin-Young Choi[4], Jea-Gun Park[4,5] and Geun Young Yeom[1,2]

[1] School of Advanced Materials Science and Engineering, Sungkyunkwan University, Suwon 16419, Republic of Korea
[2] SKKU Advanced Institute of Nano Technology (SAINT), Sungkyunkwan University, Suwon 16419, Republic of Korea
[3] Process development Team, Semiconductor R&D Center Samsung Electrics Co., Ltd., Republic of Korea
[4] MRAM Center, Department of Electronics and Computer Engineering, Hanyang University, Seoul 04763, Republic of Korea
[5] MRAM Center, Department of Nanoscale Semiconductor Engineering, Hanyang University, Seoul 04763, Republic of Korea

E-mail: gyyeom@skku.edu

Received 23 June 2020, revised 5 August 2020
Accepted for publication 18 August 2020
Published 11 November 2020

Abstract

Magnetic tunneling junction (MTJ) materials such as CoFeB, Co, Pt, MgO, and the hard mask material such as W and TiN were etched with a reactive ion beam etching (RIBE) system using H_2/NH_3. By using gas mixtures of H_2 and NH_3, especially with the H_2/NH_3 (2:1) ratio, higher etch rates of MTJ related materials and higher etch selectivities over mask materials (>30) could be observed compared to those etching using pure H_2 (no etching) and NH_3. In addition, no significant chemical and physical damages were observed on etched magnetic materials surfaces and, for CoPt and MTJ nanoscale patterns etched by the H_2/NH_3 (2:1) ion beam, highly anisotropic etch profiles >83° with no sidewall redeposition could be observed. The higher etch rates of magnetic materials such as CoFeB by the H_2/NH_3 (2:1) ion beam compared to those by H_2 ion beam or NH_3 ion beam are believed to be related to the formation of volatile metal hydrides (MH, M = Co, Fe, etc) through the reduction of M-NH_x ($x = 1 \sim 3$) formed in the CoFeB surface by the exposure to NH_3 ion beam. It is believed that the H_2/NH_3 RIBE is a suitable technique in the etching of MTJ materials for the next generation nanoscale spin transfer torque magnetic random access memory (STT-MRAM) devices.

Supplementary material for this article is available online

Keywords: reactive ion beam etching (RIBE), magnetic random access memory (MRAM), magnetic tunnel junction (MTJ), x-ray photoelectron spectroscopy (XPS), H_2, NH_3

(Some figures may appear in colour only in the online journal)

1. Introduction

Magnetic random access memory (MRAM) devices, which are non-volatile memory devices storing information by the tunneling magneto resistive (TMR) effect in the magnetic tunneling junction (MTJ), are some of the most promising candidates for the next generation memory devices due to many advantages such as high density storage, fast switching speed,

high endurance, and low power consumption [1–4]. Among these, spin transfer torque MRAM (STT-MRAM) has been the subject of intensive investigations due to its structure, which is suitable for stacking MRAM on chips to achieve higher densities at a lower cost.

The main component of the STT-MRAM device is the MTJ cell, which is consisted of a free ferromagnetic layer, a fixed ferromagnetic layer, and a tunnel barrier layer [3]. The ferromagnetic layers are the materials such as CoFeB and CoPt with high magnetic properties, and MgO is generally used as an intermediate tunnel barrier layer, therefore, a basic MTJ cell is composed of CoFeB/MgO/CoFeB, CoPt/MgO/CoPt, etc [4]. The etching of the ferromagnetic layer such as CoFeB and CoPt with halogen gases by reactive ion etching (RIE) has been previously reported. However, the etching of magnetic films with halogen gases tends to form non-volatile corrosive etch byproducts including sidewall redeposition, and which causes a tapered profile, corrosion, and electrical short [5, 6]. To solve these issues, RIE using C, H, O-based gases such as CH_3COOH/Ar, CH_3OH, CO/NH_3, etc have been investigated owing to noncorrosive property of etching and the formation of potentially volatile etch compounds [5–8]. However, oxygen in the gas mixture could induce chemical damages on the MTJ material surface during the etching and also could form a thin oxide layer on the patterned sidewall of MTJ materials, which reduces the performance of the device [9, 10].

To avoid chemical damage, RIE or ion beam etching (IBE) using inert gas such as Ar has been reported, but it has issues including sidewall redeposition and low etch selectivity with mask materials due to physical sputtering [11]. For the IBE, to remove the sidewall residue and to obtain a vertical etch profile, a tilted ion milling process has been also applied [6, 12]. However, the tilting of the ion beam is limited to the etching of low density MRAM cells because the tilting of ion beam can induce a shadow effect caused by adjacent cells, especially, in the case of high density MRAM devices required for next generation STT-MRAM devices. Therefore, reactive ion beam etching (RIBE) processes using reactive gases such as CO/NH_3 instead of Ar have been investigated and, by using the RIBE without tilting the ion beam, anisotropic etch profiles of MTJ without sidewall residues could have been observed [13, 14]. However, due to the use of the etch gas mixture containing oxygen, a possibility of chemical damages on the MTJ material surface during the etching and a thin oxide layer on the patterned sidewall of MTJ material still remains.

Therefore, in this study, to reduce the chemical damage caused by oxygen in the etch gas mixture and to improve etch profile of MTJ, the RIBE processes using reactive gas mixtures of H_2/NH_3 not containing oxygen and those using Cl_2 as a comparison have been investigated and the effects of the gas mixture on the etch characteristics of CoFeB, CoPt, TiN, W, etc and the etch profiles of MTJ were investigated. In addition, a possible etch mechanism of magnetic materials by H_2/NH_3 RIBE has been also investigated. The results showed that, by using H_2/NH_3, a highly anisotropic etch profile of MTJ without formation of a sidewall residue and a high etch selectivity over mask materials such as TiN and W could be observed without significant chemical damage of MTJ materials.

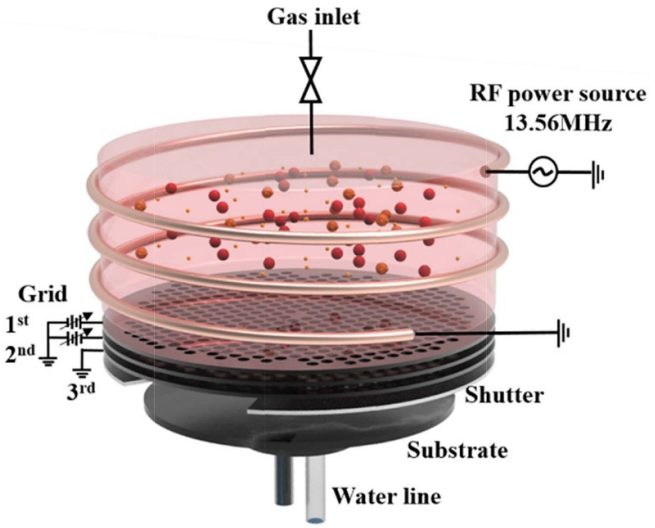

Figure 1. Schematic diagram of the reactive ion beam etch system with three-grid assembly and ICP-type plasma source used in the experiment.

2. Experimental

MRAM materials such as Co, Pt, and CoFeB, electrode/hard mask materials such as TiN and W were sputter deposited on SiO_2/Si wafers for the measurement of etch characteristics of magnetic materials using RIBE. In addition, CoPt (25 nm) and a MTJ structure of CoPt (10 nm)/MgO (1 nm)/CoFeB (10 nm)/Ta (5 nm) deposited on SiO_2/Si wafers and dot-patterned with W (86 nm)/Ru (5 nm) were used to observe the etch profiles.

The schematic drawing of the reactive ion beam etcher used in this experiment is shown in figure 1. As shown in figure 1, the reactive ion beam source was composed of an inductively coupled plasma (ICP) source operated with 13.56 MHz RF power for reactive plasma generation and a three-grid system made of graphite for the extraction and acceleration of reactive ion beam. For the reactive ion beam extraction, a positive voltage was applied to the 1st grid in contact with the plasma for the control of the ion beam energy, a negative voltage was applied to the second grid for the acceleration of the ion beam, and third grid facing the substrate was grounded. The substrate was located 10 cm below the ion beam source and maintained at room temperature. The base pressure of the process chamber was lower than 5×10^{-6} Torr, and the etching was performed at 3 mTorr of operating pressure with Cl_2 and gas mixtures of H_2/NH_3.

The energy and energy distribution of the ion beams used in the experiment was measured using a home-made retarding grid ion energy analyser equipped with a current meter (Keithley 2400) and voltage meter (Hewlett Packard 34401 A). A surface profilometer (Tencor Alpha-step 500) was used to measure the etch depth of the materials and, also, the etch rates

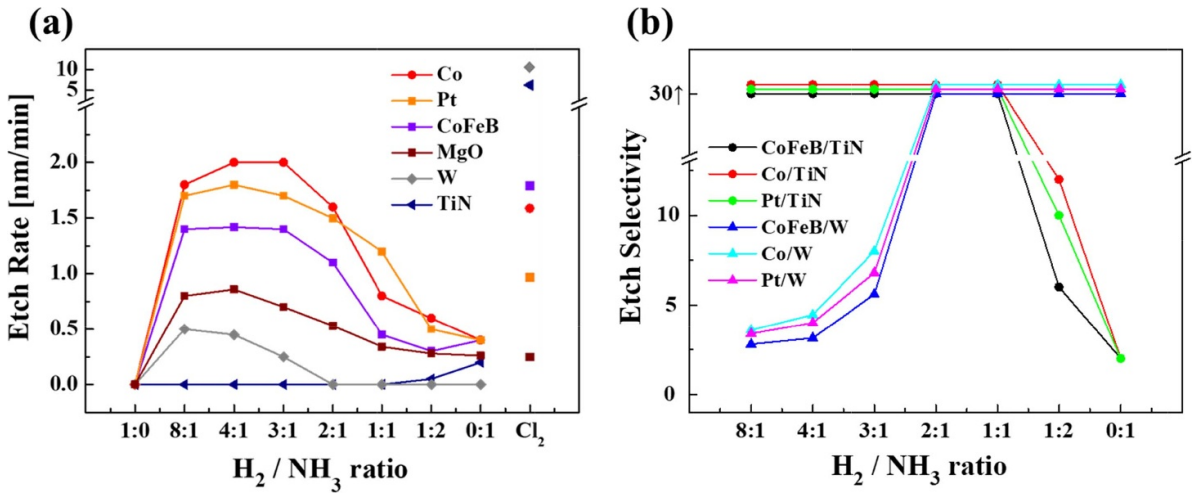

Figure 2. (a) Etch rates of magnetic materials such as Co, Pt, and CoFeB, a barrier material of MgO, and hard mask materials such as W and TiN as a function of H_2/NH_3 etch gas ratio. In comparison, the etch rates of Co, Pt, CoFeB, TiN, and W etched by Cl_2 using the same other process conditions are also shown. (b) Etch selectivities of Co, Pt, and CoFeB over hard mask materials for different H_2/NH_3 gas ratio.

and etch profiles were observed using a field emission scanning electron microscope (FE-SEM, Hitachi S-4700) after the RIBE. Also, a field emission transmission electron microscopy (FE-TEM; JEOL, JEM-F200) was used to observe the potential etch residue on the sidewall of the etched features. The surface composition and chemical binding states of magnetic materials after the etching were observed using x-ray photoelectron spectroscopy (XPS, Thermo VG, MultiLab 2000, Mg Kα source) and the surface roughness of the magnetic materials before and after the etching was observed using atomic force microscopy (AFM, Bruker Innova). A secondary ion mass spectroscopy (SIMS, TOF-SIMS-5) was also used to observe the depth of etchant species penetrated into the magnetic materials.

3. Results and discussion

3.1. Etch rate and selectivity

The etch rates of various STT-MRAM related materials such as Co, Pt, CoFeB, MgO, W, and TiN for different H_2/NH_3 ratios in the reactive ion beam are shown in figure 2(a). For the ion beam, the 1st grid voltage was maintained at +200 V, the 2nd grid voltage was at −250 V, and the 3rd grid was grounded. At this voltage condition, the ion energy was in the range of $+198 \sim 207$ eV. (The actual ion energies observed for different 1st grid voltages for $H_2/NH_3 = 2{:}1$ are shown in the Supplementary Information (figure S1 (http://stacks.iop.org/NANO/32/055301/mmedia))). As shown in figure 2(a), when pure H_2 was used, all the materials were not etched and, when pure NH_3 was used, the etch rates of <0.5 nm min^{-1} were observed for Co, Pt, CoFeB, MgO, and TiN while no etching was observed for W. However, for gas mixtures of H_2/NH_3, the increased etch rates of magnetic materials such as Co, Pt, CoFeB, and MgO with the increase of H_2/NH_3 ratio, the maximum etch rates at the ratio from 4:1 to 3:1, and the decreased etch rates with the further increase of the H_2/NH_3 ratio were observed. In the case of W, the etch rates were increased with the increase of H_2/NH_3 ratio in the gas mixture except for pure H_2 and, for TiN, the etch rate of 0.2 nm min^{-1} was observed with pure NH_3 and the increase of H_2/NH_3 ratio in the gas mixture decreased the etch rate of W and no etching of W was observed when the ratio was higher than 1:1.

In figure 2(b), the etch selectivities of Co, Pt, and CoFeB over W and TiN are shown for the conditions in figure 2(a). Even though the etching was conducted for 40 min, no noticeable etching of W and TiN observed in some H_2/NH_3 ratios, such as the H_2/NH_3 ratios from 0:1 to 2:1 for W and the ratios from 1:1 to 1:0 for TiN. Therefore, for these H_2/NH_3 ratios, the very high etch selectivities of >30 are believed to be obtained for Co, Pt, and CoFeB. Among the H_2/NH_3 ratios, the H_2/NH_3 ratio of 2:1 shows the high etch selectivity of Co, Pt, and CoFeB over both W and TiN, therefore, this H_2/NH_3 ratio was used as the following process conditions for the comparison with other etch gases such as Cl_2 and CO/NH_3 (1:3). In figure 2(a), the etch rates of CoFeB, Co, and Pt etched by Cl_2 using the same other conditions in figure 2(a) are also shown and the etch rates were 1.8, 1.6, and 1.0 nm min^{-1}, respectively. Therefore, the etch rates by Cl_2 were similar or a little higher than those by H_2/NH_3 (2:1) but the etch selectivities over W and TiN were lower than 0.3. The comparison of etch rates of CoFeB, Co, Pt, and MgO by H_2/NH_3 (2:1) with those by CO/NH_3 (1:3) using the same other conditions in figure 2(a) is also shown in Supplementary Information (figure S2) and higher etch rates of CoFeB, Co, Pt, and MgO and possibly higher etch selectivities over W and TiN were also observed for H_2/NH_3 (2:1).

3.2. XPS analysis

The surface binding states of CoFeB after the etching using H_2/NH_3 (2:1) and Cl_2 were observed using XPS. Figures 3(a), (b) and (c) show the XPS narrow scan data of Co, Fe, and Co on CoFeB, respectively, before (that is, the reference) and

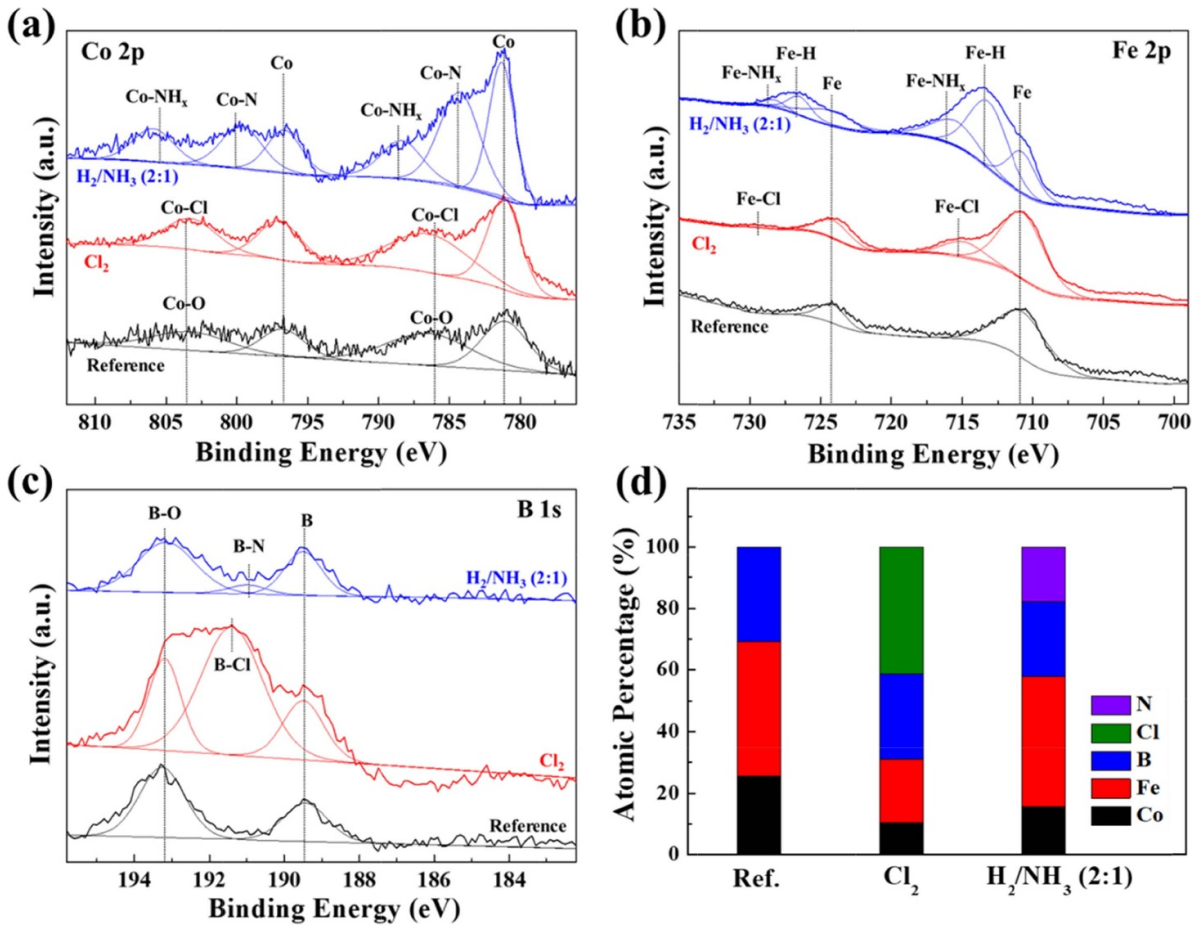

Figure 3. XPS narrow scan data of (a) Co 2p, (b) Fe 2p, (c) B 1s, and (d) relative atomic percentages of the CoFeB surface before and after the etching using reactive ion beam with H_2/NH_3 (2:1) and Cl_2 while keeping the 1st grid voltage at +200 V, 2nd grid voltage at −250 V, and 3rd grid grounded.

after the etching using H_2/NH_3 (2:1) and Cl_2. The other etch conditions are the same as those in figure 2. Also, the composition of CoFeB surface observed before and after the etching using H_2/NH_3 (2:1) and Cl_2 was also measured and the result is shown in figure 3(d). As shown in figures 3(a), (b) and (c), the surface of reference CoFeB was partially oxidized. Co showed Co−O bonding peaks at 786.8 and 803.5 eV in addition to Co peaks at 781.1 ($2p_{3/2}$) and 797 ($2p_{1/2}$) eV, and boron also showed B−O binding peaks at the 193.3 eV in addition to boron peak at 189.5 (1 s) eV while Fe showed no oxidized peak in addition to Fe peak at 711 ($2p_{3/2}$) and 724.3 ($2p_{1/2}$) eV. After the etching using Cl_2, the peaks at 786.8 and 803.5 eV similar to those of Co−O binding peaks in addition to Co peaks were observed and, due to the similar peak positions of Co−O and Co−Cl [15], it is believed that, Co−Cl binding peaks were formed instead of Co−O binding after the etching using Cl_2. In the case of Fe, after the etching using Cl_2, additional peaks at 715.1 and 729.2 eV related to Fe−Cl binding were observed [16] and, for boron, the additional peaks at 192.4 eV related to B−Cl_x binding were observed [17]. In the case of the etching using H_2/NH_3 (2:1), the additional binding peaks at 784.1 and 799.8 eV related to Co−N [18] and 788.6 and 805.6 eV peaks related to Co-NH_x binding (see Supplementary Information figure S3) were observed. For Fe, after the etching using H_2/NH_3 (2:1), additional peaks at 713.2 and 726.6 eV related to Fe−H binding and peaks at 716 and 728.3 eV related to Fe−NH_x binding could be also found (see Supplementary Information figure S3). For Boron, after the etching using H_2/NH_3 (2:1), the peaks are similar to those of the reference but a small additional peak at 190.9 eV related to B−N binding was observed [19]. In fact, a B−O binding peak was observed not only on the CoFeB sample etched by H_2/NH_3(2:1) and Cl_2 but also on the reference CoFeB sample, therefore, it is believed that the B−O binding peak observed after the etching is related to the air exposure after the etching. Therefore, after the etching using Cl_2 or H_2/NH_3 (2:1), a chemically modified surface layer was formed on the CoFeB surface. When the atomic percentages of the modified surface layer were compared, the ratio of Co:Fe:B of the reference was 25.4:43.8:30.8%, however, the ratio was changed significantly after the etching by Cl_2 by showing Co:Fe:B:Cl = 10.4:20.7:27.8:41.1% (the ratio of Co:Fe:B was 17.7:53.1:47.2%) while the ratio of Co:Fe:B:N after the etching using H_2/NH_3 (2:1) was 15.6:42.4:24.3:17.7% (the ratio of Co:Fe:B was 19:51.5:29.5%). Therefore, by the etching using H_2/NH_3 (2:1) compared to Cl_2, the impurity percentage was lower and the ratio between Co:Fe:B was closer to that of the reference.

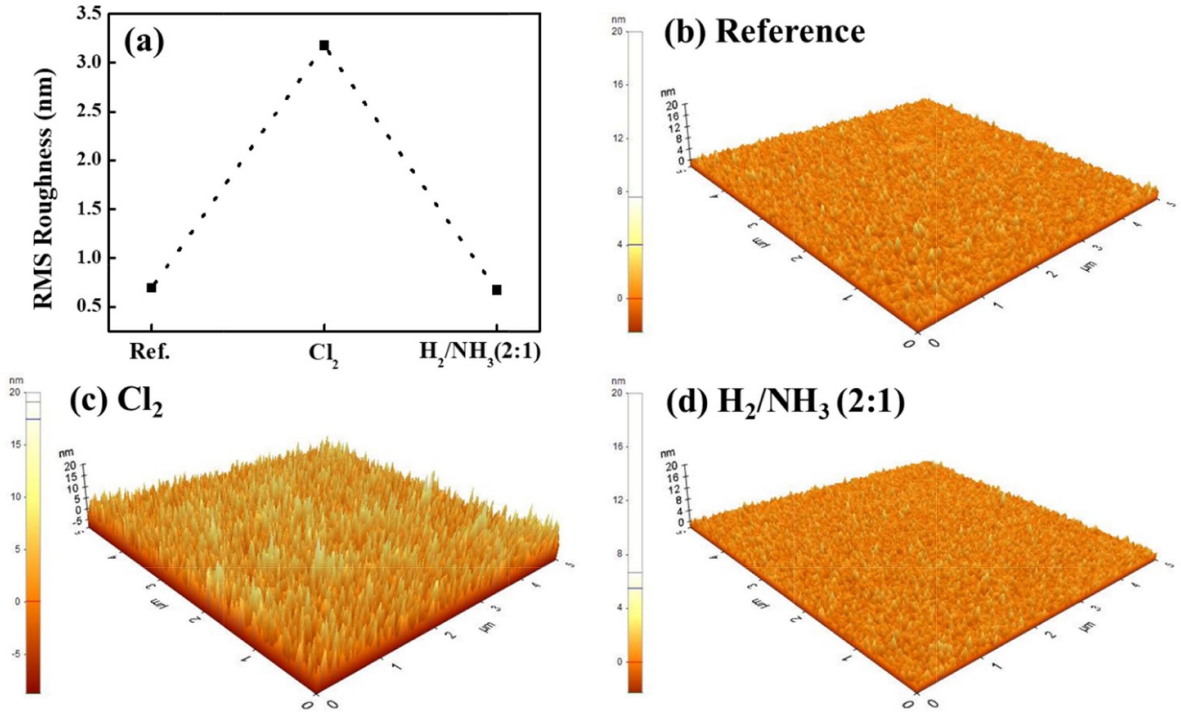

Figure 4. (a) RMS surface roughness values and 2D surface roughness images of CoFeB for (b) reference, (c) after Cl_2 etching, and (d) after H_2/NH_3 (2:1) etching for 10 min.

3.3. AFM analysis

The surface roughness values of CoFeB before and after the etching using Cl_2 and H_2/NH_3 (2:1) were compared and figures 4(a) and (b) shows the RMS surface roughness value and its image of 5 μm $\times$ 5 μm size CoFeB, respectively, before and after the etching using the etch condition in figure 2 for 10 min. As shown in figures 4(a) and (b), before the etching, the RMS surface roughness of CoFeB was $\sim$0.69 nm and, after the etching using Cl_2 ion beam, the RMS surface roughness was increased to $\sim$3.17 nm possibly due to the formation of nonvolatile chlorides such as Co$-$$Cl_x$ (B.P. of Co-Cl_2: 1049 °C) and Fe$-$$Cl_x$ (B.P. of Fe-Cl_3: 316 °C) formed on the etched CoFeB surface. However, after the etching using H_2/NH_3 (2:1), even though a modified surface layer was observed as shown in figure 3, the RMS surface roughness was $\sim$0.67 nm, therefore, the RMS surface roughness close to the reference was obtained after the etching using H_2/NH_3 (2:1) possibly due to the volatile compound formation during the RIE using H_2/NH_3 (2:1).

3.4. Etch profile and TEM analysis

In addition, CoPt (CoPt 25 nm) and a MTJ (composed of CoPt (10 nm)/MgO (1 nm)/CoFeB (10 nm)/Ta (5 nm)) on SiO_2 patterned with a W (86 nm)/Ru (10 nm) hard mask were etched using the conditions in figure 2(a) with H_2/NH_3 (2:1) and Cl_2 ion beams and the etch profiles were observed using SEM and the results are shown in figures 5(a) and (b) for the CoPt and figures 5(c) and (d) for the MTJ layer. As shown in figures 5(a) and (c), for the etching using H_2/NH_3 (2:1) ion beam, highly anisotropic etch profiles of CoPt ($\sim$85°) and MTJ ($\sim$84°) layers without significantly etching the W dot pattern could be observed due to the very high etch selectivity of magnetic materials over W and TiN as shown in figure 2(a) while CoPt and MTJ etched using Cl_2 showed the significant etching of the W hard mask layer due to the low etch selectivity, therefore, the etch profiles were completely ruined. To observe the sidewall residue on the etched CoPt and MTJ layers, the CoPt and MTJ etched with H_2/NH_3 (2:1) in figures 5(a) and (c) were also observed by TEM and the results are shown in figure 6. As shown in figure 6, the sidewalls of CoPt and MTJ etched structures were clean, therefore, no sidewall residues appear to be formed on the sidewall of the etched CoPt and MTJ.

3.5. Etch mechanism

The high etch rates of magnetic materials, no increase of surface roughness after the etching, and no sidewall residue observed with H_2/NH_3 (2:1) IBE appear to be related to the formation of volatile etch products during the etching using H_2/NH_3 ion beam. To figure out a potential etch mechanism, the CoFeB was etched by a cyclic etching both by one step continuous etching using NH_3 ion beam (1 min etching) per cycle and by two step etching composed of NH_3 ion beam (1 min etching) $\rightarrow$ H_2 ion beam (0 $\sim$ 5 min) per cycle and their etch characteristics were compared and the results are shown in figure 7. (For the cyclic etch experiment, due to the low etch rate (<0.5 nm min^{-1}) of CoFeB with the NH_3 ion beam, a lower operating pressure of 1 mTorr instead of 3 mTorr was used for NH_3 ion beam to increase the etch rate of CoFeB while other process conditions are kept the same, and the higher etch rate ($\sim$1.5 nm min^{-1})

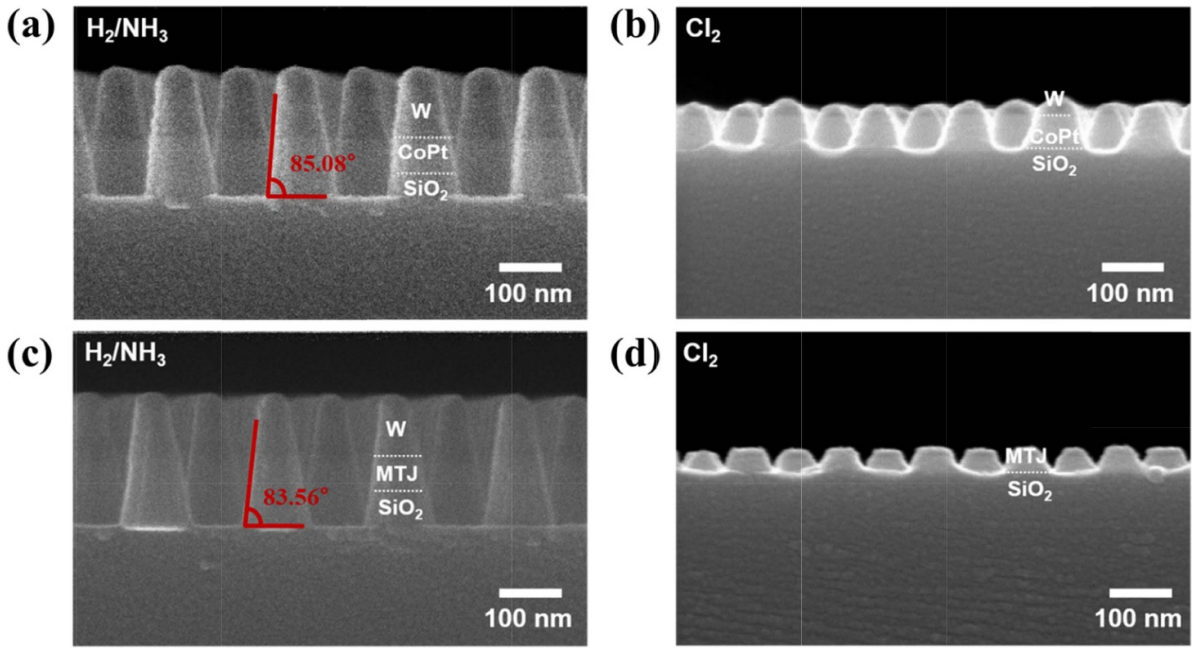

Figure 5. SEM etch profiles of CoPt (a, b) and MTJ (CoPt/MgO/CoFeB)/Ta (c, d) on SiO_2 patterned with a W/Ru hard mask. CoPt and MTJ were etched using (a, c) H_2/NH_3 (2:1) and (b, d) Cl_2 ion beams.

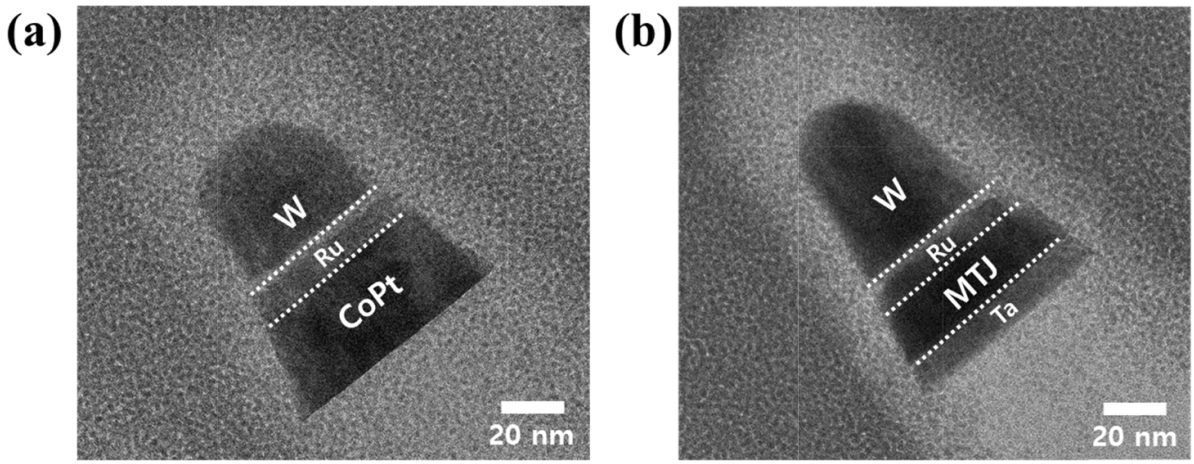

Figure 6. FE-TEM images of (a) CoPt and (b) MTJ (CoPt/MgO/CoFeB)/Ta on SiO_2 patterned with a W/Ru hard mask for (a) and (c) in Figure 5.

of CoFeB was obtained with the 1 mTorr NH_3 ion beam. But, for the H_2 ion beam, due to the difficulty in sustaining the H_2 plasma at 1 mTorr, the H_2 ion beam operated at 3 mTorr was used for the cyclic etching experiment. For H_2/NH_3 (2:1), at 1 mTorr of operating pressure, the etch rate of CoFeB was also increased to 3.4 nm min^{-1} from 1.1 nm at 3 mTorr.) figure 7(a) shows XPS N1s narrow scan peaks on the CoFeB after the 1 min NH_3 IBE and after 1 min NH_3 IBE (1 mTorr) $\rightarrow$ 2 min H_2 IBE (3 mTorr). As shown in figure 7(a), when CoFeB was etched using NH_3, peaks related to N (398.3 eV), NH_2/NH (399.4 eV), NH_3^+ (401.5 eV), and NO_2 (405 eV) were observed on the etched CoFeB surface due to the modification of the CoFeB by the NH_3 ion beam. However, most of those peak intensities were removed after the 2 min H_2 IBE. As shown in figure 7(b), the nitrogen percentage of the CoFeB surface after the etching using NH_3 ion beam for 1 min was about 15.5%, however, the after the exposure to H_2 ion beam for 2 min, the nitrogen percentage on the etched CoFeB surface was significantly decreased to 2.5%. It is believed that the decrease of N-related peaks such as NH/NH_2, NH_3^+, etc on the CoFeB surface is related to the etching of CoFeB by forming a hydride such as CoH, FeH, BH_x on the surface during the exposure to H_2 ion beam.

Figure 7(c) shows the etch depth of CoFeB with the increase of etch cycles by cyclic etching with one step continuous etching using NH_3 ion beam (1 min) per cycle, with one step continuous etching using H_2 ion beam (2 min) per cycle, and with two step etching composed of NH_3 ion beam (1 min) $\rightarrow$ H_2 ion beam (0 $\sim$ 5 min) per cycle. As shown in figure 7(c), when CoFeB was etched with one step continuous

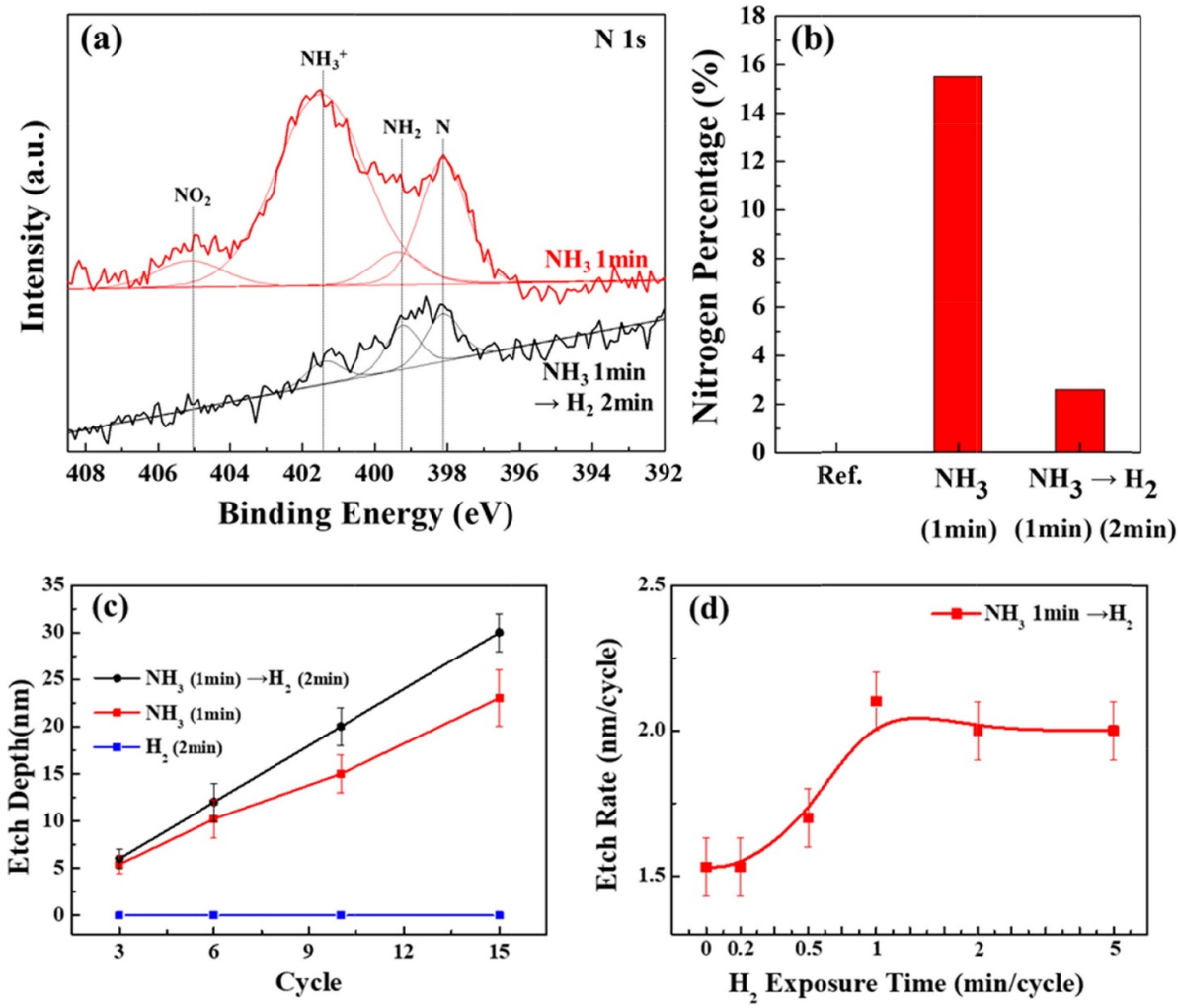

Figure 7. CoFeB etch mechanism using $NH_3 \rightarrow H_2$ cyclic ion beam etching. (a) XPS N1s narrow scan peaks on the CoFeB after the 1 min NH_3 ion beam etching and after 1 min NH_3 ion beam etching → 2 min H_2 ion beam etching. (b) Relative atomic percentages of nitrogen on CoFeB of figure 7(a). (c) Etch depth of CoFeB with the increase of etch cycles by cyclic etching with one step continuous etching using NH_3 ion beam (1 min) per cycle, with one step continuous etching using H_2 ion beam (2 min) per cycle, and with two step etching composed of NH_3 ion beam(1 min) → H_2 ion beam (2 min) per cycle. (d) CoFeB etch depth/cycle as a function of H_2 exposure time in the two step cyclic etching composed of NH_3 ion beam (1 min) → H_2 ion beam. To obtain a higher CoFeB etch rate with NH_3 ion beam from ∼0.5 to 1.53 nm min^{-1}, a low operating pressure of 1 mTorr instead of 3 mTorr was used in this experiment.

etching using H_2 ion beam (2 min) per cycle, no etching of CoFeB was observed similar to the results on CoFeB etching using H_2 ion beam in figure 2(a). Also, when CoFeB was etched with one step continuous etching using NH_3 ion beam (1 min) per cycle, 1.53 nm min^{-1} was observed. However, when the CoFeB was etched with two step etching composed of NH_3 ion beam (1 min) → H_2 ion beam (2 min) per cycle, the etch depth per cycle was increased ∼30% compared to that etched with one step NH_3 only, therefore, ∼2 nm/cycle was obtained as shown in figure 7(c).

To understand the effect of H_2 ion beam for the two step etching composed of NH_3 ion beam (1 min) → H_2 ion beam, the H_2 ion beam exposure time was varied from 0 to 5 min/-cycle after the NH_3 IBE for 1 min and the result is shown in figure 7(d). By increasing the H_2 exposure time, the etching by the H_2 exposure was increased, however, it was saturated at ∼0.5 nm/cycle at ∼1 min exposure to H_2 ion beam and the further exposure to H_2 ion beam did not etch the CoFeB further. Therefore, the H_2 ion beam exposure to CoFeB etched using NH_3 ion beam removed the saturated CoFeB thickness of ∼0.5 nm per cycle. When the surface of CoFeB etched with NH_3 ion beam for 1 min was observed using SIMS, the penetration of NH_x less than ∼1 nm into CoFeB could be observed (Supplementary Information figure S4). The NH_x penetrated in the CoFeB etched by NH_3 ion beam will exist in the CoFeB as the form of $M-NH_x$ ($x = 1 \sim 3$, M = Co, Fe) as can be seen in XPS surface analysis in figures 3(a) and (b). Therefore, it is believed that, during the two step etch cycle, the ∼0.5 nm thick CoFeB after the etching using NH_3 ion beam was further etched by forming volatile hydrides of M−H(g) from $M-NH_x$ similar to the formation of volatile M−H(g) from $M-Cl_x$ (M = Co, Fe, Ni, etc) observed during the magnetic mater-

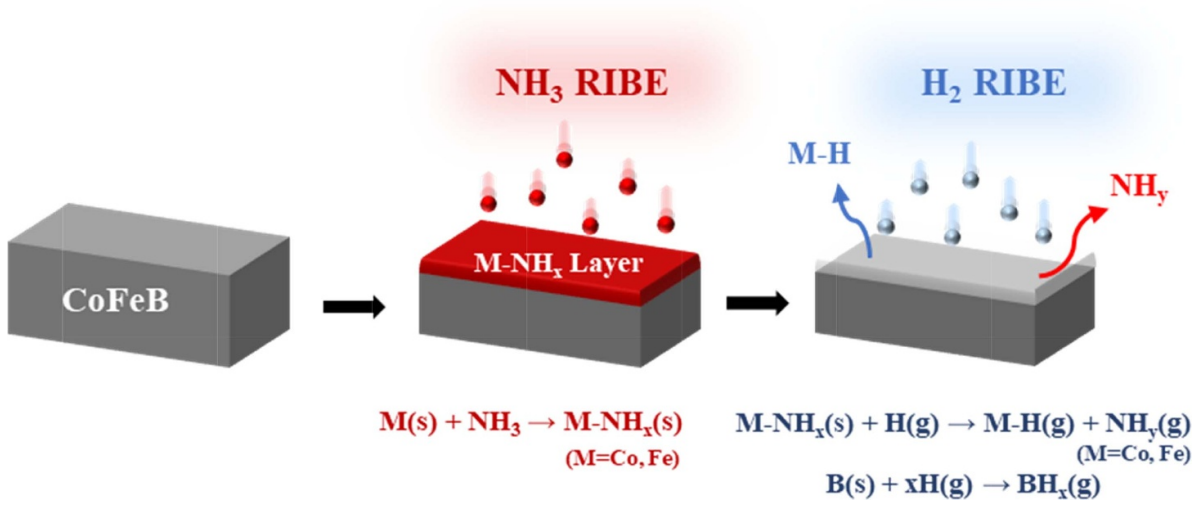

Figure 8. Possible reaction mechanism on the etching of CoFeB with H_2/NH_3 ion beam.

ial two step cyclic etching using Cl_2 plasma $\rightarrow$ H_2 plasma [15, 20]. Figure 8 shows the possible magnetic material etch mechanism during the etching of H_2/NH_3 (2:1) or during the two step cyclic etching composed of NH_3 ion beam $\rightarrow$ H_2 ion beam, that is,

$M(s) + NH_x(g)$ (by NH_3 ion beam) $\rightarrow M{-}NH_x(s)$

$M{-}NH_x(s) + yH(g)$ (by H_2 ion beam) $\rightarrow M{-}H(g) + NH_3(g)$

$B(s) + xH(g) \rightarrow BH_x(g)$

where, M is Co, Fe, etc, $x = 1 \sim 3$, $y = 1 \sim 2$. Therefore, it is believed that, through formation of volatile magnetic hydrides (MH(g)) from the $M{-}NH_x$, high etch rates, smooth surface, and less surface impurity for the etching of magnetic materials were obtained for $H_2{:}NH_3$ (2:1) ion beam.

4. Conclusions

In this study, MTJ related materials such as CoFeB, Co, Pt, MgO and hard mask materials such as TiN, W were etched using RIBE using H_2/NH_3 gases for more selective and more anisotropic etching of nanoscale MTJ stack with less sidewall residue for MRAM devices. The etch rates of MTJ related materials and their etch selectivities over mask materials by H_2/NH_3 (2:1) ion beam were higher compared to those by pure H_2 ion beam and NH_3 ion beam. In addition, the use of H_2/NH_3 ion beam exhibited no significant chemical and physical damage on magnetic materials such as CoFeB surface. Due to the high etch selectivity over mask materials, the etching of MTJ and CoPt patterned with a W hard mask using H_2/NH_3 ion beam exhibited a highly anisotropic etch profile >83°. Also no sidewall redeposition on CoPt and MTJ patterns etched by the H_2/NH_3 (2:1) ion beam was observed. The higher etch rates of magnetic materials such as CoFeB by the H_2/NH_3 (2:1) ion beam compared to those by H_2 ion beam or NH_3 ion beam are believed to be related to the formation of volatile metal hydrides (MH, M = Co, Fe, etc) through the reduction of $M{-}NH_x$ ($x = 1 \sim 3$) formed in the CoFeB surface by the exposure to NH_3 ion beam.

Acknowledgments

This work is supported by the Samsung Electronics' university R&D program. [Development of small pitch MTJ patterning process using RIBE].

ORCID iDs

Jea-Gun Park https://orcid.org/0000-0002-5831-2854
Geun Young Yeom https://orcid.org/0000-0001-6603-2193

References

[1] Comstock R L 2002 Review modern magnetic materials in data storage *J. Mater. Sci., Mater. Electron.* **13** 509–523
[2] Kishi T *et al* 2008 Lower-current and fast switching of a perpendicular TMR for high speed and high density spin-transfer-torque MRAM *2008 IEEE Int. Electron Devices Meeting*, *San Francisco* CA 1–4
[3] Kent A D and Worledge A C 2015 A new spin on magnetic memories *Nat. Nanotechnol.* **10** 187–91
[4] Ikeda S, Miura K, Yamamoto H, Mizunuma K, Gan H D, Endo M, Kanai S, Hayakawa J, Matsukura F and Ohno H 2010 A perpendicular-anisotropy CoFeB–MgO magnetic tunnel junction *Nat. Mater.* **9** 721–4
[5] Park J Y, Kang S K, Jeon M H, Jhon M S and Yeom G Y 2011 Etching of CoFeB Using CO/NH3 in an inductively coupled plasma etching system *J. Electrochem. Soc.* **158** 1–4
[6] Peng X, Wakeham S, Morrone A, Axdal S, Feldbaum M, Hwu J, Boonstra T, Chen Y and Ding J 2009 Towards the sub-50 nm magnetic device definition: ion beam etching (IBE) vs plasma-based etching *Vacuum* **83** 1007–13
[7] Otani Y, Kubota H, Fukushima A, Maehara H, Osada T, Yuasa S and Ando K 2007 Microfabrication of magnetic tunnel junctions using CH_3OH etching *IEEE Trans. Magn.* **43** 2776–8
[8] Garay A A, Hwang S M, Choi J H, Min B C and Chung C W 2015 Inductively coupled plasma reactive ion etching of CoFeB magnetic thin films in a CH_3COOH/Ar gas mixture *Vacuum* **119** 151–8

[9] Sugiura K *et al* 2009 Ion beam etching technology for high-density spin transfer torque magnetic random access memory *Jpn. J. Appl. Phys.* **48** 08HD02
[10] Kinoshita K, Yamamoto T, Honjo H, Kasai N, Ikeda S and Ohno H 2012 Damage recovery by reductive chemistry after methanol-based plasma etch to fabricate magnetic tunnel junctions *Jpn. J. Appl. Phys.* **51** 08HA01
[11] Kim E H, Lee T Y and Chung C W 2012 Evolution of etch profile of magnetic tunnel junction stacks etched in a CH_3OH/Ar plasma *J. Electrochem. Soc.* **159** H230–H234
[12] Jeong J and Endoh T 2017 Ion beam etching process for high-density spintronic devices and its damage recovery by the oxygen showering post-treatment process *Jpn. J. Appl. Phys.* **56** 04CE09
[13] Jeon M H, Yang K C, Park J W, Yun D H, Kim K N and Yeom G Y 2015 Etch residue removal of CoFeB using CO/NH_3 reactive ion beam for spin transfer torque-magnetic random access memory device *J. Vac. Sci. Technol.* **33** 061212
[14] Jeon M H, Yang K C, Park J W, Yun D H, Kim K N and Yeom G Y 2016 Etching of magnetic tunnel junction materials using reactive ion beam *J. Nanosci. Nanotechnol.* **16** 11823–30
[15] Kim T, Chen J and Chang J P 2014 Thermodynamic assessment and experimental verification of reactive ion etching of magnetic metal elements *J. Vac. Sci. Technol.* **32** 041305
[16] Thermo Scientific. XPS Simplified: iron https://xpssimplified.com/elements/iron.php
[17] Shamiryan D, Baklanov M, Claes M, Boullart W and Paraschiv V 2009 Selective removal of high-kgate dielectrics *Chem. Eng. Comm.* **196** 1475–535
[18] Zhong H, Tian R, Gong X, Li D, Tang P, Vante N A and Feng Y 2017 Advanced bifunctional electrocatalyst generated through cobalt phthalocyanine tetrasulfonate intercalated Ni2Fe-layered double hydroxides for a laminar flow unitized regenerative micro-cell *J. Power Sources* **361** 21–30
[19] Sudeep P M, Vinod S, Ozden S, Sruthi R, Kukovecz A, Konya Z, Vajtai R, Anantharaman M R, Ajayan P M and Narayanan T N 2015 Functionalized boron nitride porous solids *RSC Adv.* **5** 93964–8
[20] Altieri D N and Chang J P 2018 Atomic layer etching of magnetic and noble metals *UCLA Electronic Theses and Dissertations*